

Squeezed Displaced Schrödinger-cat state as a signature of the \mathcal{PT} -symmetry phase transition

Yuetao Chen, Shoukang Chang, and Shaoyan Gao*

MOE Key Laboratory for Nonequilibrium Synthesis and Modulation of Condensed Matter,
Shaanxi Province Key Laboratory of Quantum Information and Quantum Optoelectronic Devices,
School of Physics, Xi'an Jiaotong University, 710049, People's Republic of China.

Parity-time (\mathcal{PT}) symmetric systems are gain-loss systems whose dynamics are governed by non-Hermitian Hamiltonians with degeneracies at exceptional-points (EPs) and has been studied in various photonic, electrical, mechanical systems, and so on. However, it is still an open question how to capture \mathcal{PT} symmetry phase transition in electronic system where the transport properties of electron will be dramatically effected. Fortunately, the hybridization between photon and electron offers a novel way not only to control but also probe material properties. Here, we investigate a cavity coupled to a non-Hermitian Su-Schrieffer-Heeger (SSH) chain within mean-field ansatzs. We find that Squeezed Displaced Schrodinger cat (SDSc) will emerge with high fidelity in cavity ground state when \mathcal{PT} -symmetry is broken and the fidelity will experience a sharp drop from almost 1 to 0 as \mathcal{PT} symmetry recovers. Additionally, in semiclassical limit, we find that there exists local extrema at two sides of $x=0$ in semiclassical photon Hamiltonian $H_{\text{eff}}(x, p)$, a clear signature of the emergence of SDSc state in cavity ground state. Thus, the appearance of SDSc state can be used to capture \mathcal{PT} -symmetry phase transition which can not be modified by cavity mode. Besides, we exploit the cavity ground state to estimate the phase in the optical interferometer, and show that the quantum Fisher information and nonclassicality will sharply decline at EPs. This reveals that \mathcal{PT} -symmetry breaking in electronic materials can also be captured by the quantum Fisher information and nonclassicality in phase estimation.

I. INTRODUCTION

The \mathcal{PT} -symmetry phase transition, as a subset of non-Hermiticity which represents a fundamental departure from conventional quantum mechanics [1–10], manifesting a transition from a real energy spectrum to a complex one. Intrinsic \mathcal{PT} -symmetry breaking spontaneously emerges at EPs where nonreciprocal hopping strength is equal to reciprocal one in a sublattices, and eigenstates and eigenvalues coincide [11–19]. The presence of EPs gives rise to rich physical phenomena, including enhancing precision in quantum sensors [20], topological phase transitions [21–25], nonadiabatic transitions [26,27], unidirectional light propagation [28], and energy transport at macroscopic [29], among others. In recent years, significant attention has been drawn to realize \mathcal{PT} -symmetry phase transition, with demonstrations in optical system [30–32], electrical system [33], and mechanical setting [34]. However, apart from the interest of realizing \mathcal{PT} -symmetry phase transition systems in various fields, probing \mathcal{PT} -symmetry breaking is still an open question, particularly in electronic systems, where such breaking can exert a significant influence on electron transport.

Fortunately, quantum Floquet presents a novel way for probing, manipulating, and fine-tuning material properties, leading for instance to the emergence of polaritons—hybrid light-matter excitations—exhibiting non-trivial topological characteristics [35–41], or to an anomalous Hall response in the presence of a circularly polarized field [42]. As the quantum version of classical Floquet engineering, quantum Floquet has been proposed to control materials through quantum light without detrimental heating [43]. The fundamental idea involves embedding a material within an optical cavity and

amplify the light-matter interaction [44, 45] due to the inverse square-root relationship between the coupling strength and the effective mode volume [45, 46]. This amplification can be achieved, for instance, through near-field enhancement effects [47]. Through this enhancement of the coupling, one can achieve the aim of classical Floquet engineering with only quantum vacuum fluctuations or a few photons in cavity. To meet the theoretical requirements, ultra-strongly coupled light-matter systems have been achieved through various implementation schemes, beginning with initial findings utilizing microwave and optical cavities [48, 49] where the properties of electronic materials can be well manipulated. Apart from controlling materials, the interaction between cavity photons and material electron also has an effect on cavity ground state, leading for example to the emergence of squeezed vacuum state [50] and displaced squeezed vacuum state [51] where cavity Hamiltonian can be renormalised by hopping parameter in hermitian electronic materials within mean-field ansatzs. Naturally, a basic question to be asked here is what is the fate of the cavity ground state coupling to electron in the presence of \mathcal{PT} -symmetry phase transition in non-Hermitian electronic materials and whether one can capture \mathcal{PT} -symmetry phase transition sensitively by a probe of cavity ground state.

In this paper, we address this fundamental question by investigating the interplay of electron and quantum light by considering the non-Hermitian electronic SSH chain coupled to a single mode cavity through the full gauge invariant Peierls phase. Electronic energy spectrum and cavity ground state can be obtained by diagonalizing electronic Hamiltonian and photon Hamiltonian within mean-field ansatzs where there is no correlation between electron and photon. From view of electronic degree, we shows that quantum fluctuations of the light field have no effect on \mathcal{PT} -symmetry phase transition but exhibit dramatic effects on the topological properties of the system which can be probed by photonic spectrum. How-

* gaosy@xjtu.edu.cn

ever, from the perspective of photon degree, the results show that Squeezed Displaced Schrödinger-cat (SDSc) state with high fieldity emerges as \mathcal{PT} -symmetry broken and then disappears immediately when \mathcal{PT} symmetry recovers. This reveals that the emergence of SDSc state can be regarded as a signature of \mathcal{PT} -symmetry phase transition in electronic materials and is possible due to the appearance of local extrema at two sides of $x=0$ in semiclassical photon Hamiltonian $H_{\text{eff}}(x, p)$.

With the cavity ground state in our scheme, we also estimate the linear phase in the optical interferometer. We find that the quantum Fisher information (QFI) about the phase and the nonclassicality of cavity ground will experience dramatic drop at EPs. Thus, QFI and the nonclassicality of cavity ground can be also regarded as signatures of \mathcal{PT} -symmetry phase transition.

This paper is organized as follows. In II, we introduce we describe the Hamiltonian of the light-matter coupled system. In III, we show the effect of quantum vacuum fluctuation in cavity on electronic spectrum in open boundary condition. In IV, we discuss about the generation of SDSc state as \mathcal{PT} -symmetry breaking and investigate the influence of \mathcal{PT} -symmetry phase transition on the fidelity between exact SDSc state and cavity ground state. Semiclassical photon Hamiltonian $H_{\text{eff}}(x, p)$ will be studied for explaining the physics behind the emergence of SDSc state. In V, we exploit the cavity ground state to estimate the phase of the optical interferometer, and study the QFI and nonclassicality of cavity ground state at two sides of EPs. Finally, VI presents the discussion and summary of the main findings in this work.

II. HAMILTONIAN

Model. We consider a 1D tight-binding non-Hermitian SSH model coupled to a single mode cavity which is pictorially shown in Fig. 1. The above model describes spin-

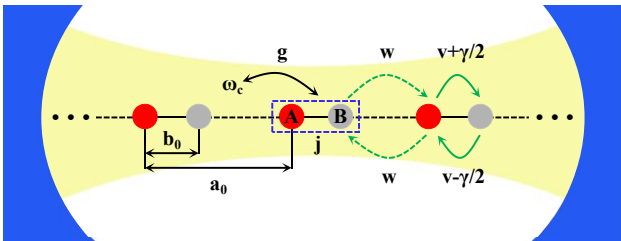


FIG. 1. **Scheme of the non-Hermitian Su-Schrieffer-Heeger chain coupled to cavity.** A one-dimensional dimerized Su-Schrieffer-Heeger chain with nonreciprocal intracell $v \pm \gamma/2$ (green solid line) and intercell w (green dashed line) hopping amplitudes coupled to a single mode cavity with frequency ω_c . The strength of the light-matter coupling is denoted by g_{coupling} . The lattice constant is given by a_0 , and the distance between the sublattices A and B within the same unit cell (depicted by the blue dashed square) is b_0 .

free electron nonreciprocal nearest-neighbor hopping in a one-dimensional chain of L units with two sublattices A and B.

The corresponding Hamiltonian is

$$H_{\text{non-Hermitian-SSH}} = (v + \frac{\gamma}{2}) \sum_{j=1}^L c_{j,A}^\dagger c_{j,B} + (v - \frac{\gamma}{2}) \sum_{j=1}^L c_{j,B}^\dagger c_{j,A} - w \sum_{j=1}^{L-1} c_{j+1,A}^\dagger c_{j,B} - w \sum_{j=1}^{L-1} c_{j,B}^\dagger c_{j+1,A}, \quad (1)$$

where $v(w)$ are lattice intracell (intercell) hopping strength and γ is the nonreciprocal intracell hopping strength, meanwhile $c_{j,\zeta}^\dagger (c_{j,\zeta})$ are the fermionic creation (annihilation) operators at site j and sublattice $\zeta = A, B$. a_0 and b_0 are the lattice constant and intracell distance between A and B sites correspondingly as shown in Fig. 1. The non-Hermitian SSH model displays topological phase transitions ($v = \pm \sqrt{w^2 + (\frac{\gamma}{2})^2}$) and \mathcal{PT} -symmetry breaking phase transitions ($v = \pm \frac{\gamma}{2}$) in the absence of any light-matter interaction. It's worth noting that the two phase transitions mentioned above are independent of the intracell distance b_0 without cavity. The Hamiltonian of the single mode cavity which is coupled to the non-Hermitian SSH model reads

$$H_{\text{phot}} = \omega_c (a^\dagger a + \frac{1}{2}), \quad (2)$$

where ω_c is the mode frequency and the single cavity mode annihilation (creation) operators are represented by $a (a^\dagger)$ satisfying the Bose-Einstein commutation relation $[a, a^\dagger] = 1$. We couple the 1D non-Hermitian SSH model to the single cavity mode by applying a unitary transformation U to electronic Hamiltonian[47], i.e.

$$H = H_{\text{phot}} + U^\dagger H_{\text{non-Hermitian-SSH}} U, \quad (3)$$

where the unitary transformation U is defined as

$$U = \exp(i e A \sum_{j,\zeta} r_{j,\zeta} c_{j,\zeta}^\dagger c_{j,\zeta}), \quad (4)$$

where $r_{j,\zeta}$ represents the position of the sublattice, with $r_{j,A} = j a_0$ and $r_{j,B} = j a_0 + b_0$. The full Hamiltonian under this transformation can be written as (setting $a_0 = 1$)

$$H = (v + \frac{\gamma}{2}) e^{i \frac{g_{\text{coupling}}}{\sqrt{L}} b_0 (a + a^\dagger)} \sum_{j=1}^L c_{j,A}^\dagger c_{j,B} + (v - \frac{\gamma}{2}) e^{-i \frac{g_{\text{coupling}}}{\sqrt{L}} b_0 (a + a^\dagger)} \sum_{j=1}^L c_{j,B}^\dagger c_{j,A} - w e^{i \frac{g_{\text{coupling}}}{\sqrt{L}} (1-b_0)(a + a^\dagger)} \sum_{i=1}^{L-1} c_{j+1,A}^\dagger c_{j,B} - w e^{-i \frac{g_{\text{coupling}}}{\sqrt{L}} (1-b_0)(a + a^\dagger)} \sum_{i=1}^{L-1} c_{j,B}^\dagger c_{j+1,A} + \omega_c (a^\dagger a + \frac{1}{2}), \quad (5)$$

where $A = \frac{g_{\text{coupling}}}{\sqrt{L}}(a + a^\dagger)$ are related to the quantized electromagnetic vector potential with the convention $e = \hbar = c = 1$. It's worth noting that the full light-matter interaction Hamiltonian obtained by applying unitary transformation is equivalent to the Hamiltonian under Peierls substitution[] where the hoppings amplitudes in Eq. (1) are dressed as $v \rightarrow v \exp(i e A b_0)$, $\gamma \rightarrow \gamma \exp(i e A b_0)$ and $w \rightarrow w \exp[-i e A (a_0 - b_0)]$. This phenomenon will play a key role in modifying the electron energy spectrum under open boundary conditions. Furthermore, the presence of non-Hermitian SSH chain will exert a discernible impact on the ground state of the cavity depending on the hopping parameters in non-Hermitian SSH chain. Strikingly, we will show that the presence of nonreciprocal hopping in non-hermitian SSH model can lead to the emergency of SDS states with high fidelity which can be regarded as a signature of the \mathcal{PT} -symmetry breaking phase transition in non-Hermitian SSH chain and have great potential for applications in quantum information processing and quantum metrology.

III. THE OPEN-BOUNDARY ENERGY SPECTRUM OF NON-HERMITIAN SSH MODEL IN THE PRESENCE OF CAVITY

The finite-length energy spectrum of the non-Hermitian SSH model exhibits a \mathcal{PT} -symmetry-breaking phase transition in the non-Hermitian SSH model due to the nonreciprocal hopping, manifested through the emergence of complex eigenenergy spectra. The other investigation we carry out is therefore what is the fate of the \mathcal{PT} symmetry with a finite coupling to the cavity mode serving as the primary focus of our inquiry. Meanwhile, there exists a distinctive signature of its non-trivial topology, the presence of exponentially localized zero modes near the boundaries. Hence, we also investigate the behavior of the zero modes in the presence of cavity. To this extent we study the model within a mean field ansatz (see appendix A) assuming that there is no entanglement between the cavity ground modes $|\phi\rangle$ and electronic ground state $|\varphi\rangle$. The renormalised non-Hermitian SSH Hamiltonian dressed by cavity obtained within this ansatz reads

$$\begin{aligned} H_{\text{non-Hermitian-SSH}}^{mf} &= \langle \phi | H | \phi \rangle \\ &= (v' + \frac{\gamma'}{2}) \sum_{j=1}^L c_{j,A}^\dagger c_{j,B} + (v' - \frac{\gamma'}{2}) \sum_{j=1}^L c_{j,B}^\dagger c_{j,A} \\ &\quad - w' \sum_{j=1}^{L-1} c_{j+1,A}^\dagger c_{j,B} - w' \sum_{j=1}^{L-1} c_{j,B}^\dagger c_{j+1,A}, \end{aligned} \quad (6)$$

where $v' = v \xi(g_{\text{coupling}}, b_0)$, $\gamma' = \gamma \xi(g_{\text{coupling}}, b_0)$ and $w' = w \xi(g_{\text{coupling}}, 1 - b_0)$ are the dressed hoppings strength by cavity with the factor

$$\xi(g_{\text{coupling}}, l) = \langle \phi | e^{-i \frac{g_{\text{coupling}}}{\sqrt{L}} l (a + a^\dagger)} | \phi \rangle. \quad (7)$$

Meanwhile, a renormalised photon Hamiltonian H_{phot} is obtained within the mean field ansatz (see Methods for the specific expression). By self-consistently solving the corresponding mean-field Hamiltonian, we obtain the photonic ground state $|\phi\rangle$ and the electronic ground state $|\varphi\rangle$, and find that the renormalization factor $\xi(g_{\text{coupling}}, l)$ is only real due to the lack of a finite current in the ground state of electron-photon coupling Hamiltonian. It's worth noting that the numerical methods employed in obtaining the ground state achieve a high level of accuracy, limited only by the cutoff of the maximum photon number in the Fock space $N_{\text{max}}^{\text{phot}}$, and we choose $N_{\text{max}}^{\text{phot}} = 60$ for accuracy and simplicity. The finite-length energy spectrum of the non-Hermitian SSH model can be obtained by orthogonalizing $H_{\text{non-Hermitian-SSH}}$ and is plotted in Fig. 2(a)-(i) as functions of lattice intracell hopping amplitude v for different values of the light-matter coupling strength g_{coupling} and intracell distance b_0 . As shown in Fig. 2(a), consistent with expectations for $g_{\text{coupling}} = 0$, we observe a TPT when $v \approx \pm 1.2$ (red dashed line). During this transition, a pair of exponentially small almost zero modes emerge within the central region of the gap in the bulk in Fig. 2(c). Meanwhile, there exists \mathcal{PT} -symmetry phase transition at EPs ($v \approx \pm 0.6$) which leads to emergence of imaginary energy spectrum as depicted in Fig. 2(b). At \mathcal{PT} symmetric region, the real part of energy spectrum in Fig. 2(c) can captures the properties of non-Hermitian SSH model. Upon considering light-matter coupling, the energy spectrum changes for different intracell distance b_0 . Especially, the TPT point (red dashed line) is shifted to smaller values of v for $b_0 = 0.2$ as shown in Fig. 2(d), revealing that the TPT of non-Hermitian SSH model can be modified by the quantum fluctuation of the cavity mode. In additional, In Fig. 2(g), it is evident that the TPT point (red dashed line) is pushed to larger values of v when $b_0 = 0.8$, and zero modes edge states can appear over a wider value range of v compared to the situation when $b_0 = 0.2$. This indicates that coupling to the quantum fluctuation of the light field can affect the TPT in the open boundary condition and this is consistent with the situation in the periodical boundary condition (see appendix B). In addition, the photonic spectral function's behavior which encoding how the light emitted from the cavity also show the TPT in the presence of cavity (see appendix C). However, unlike TPT point, EPs remain stable for different value of b_0 in Fig. 2(e) and Fig. 2(h), indicating the robustness of \mathcal{PT} -symmetry phase transition to quantum fluctuation of cavity mode. However, the ground state of cavity will experience a sharp change when the \mathcal{PT} symmetry of the non-Hermitian SSH model is broken, as we are going to discuss below.

IV. THE GENERATION OF SQUEEZED DISPLACED SCHRÖDINGER-CAT STATES

As is known to all, the photon groundstate of a pure cavity is vacuum state where there only exists vacuum fluctuations without any photon. However, different photon groundstate will emerge by considering the interaction between an one-dimension electronic chain and cavity mode. Hence, we in-

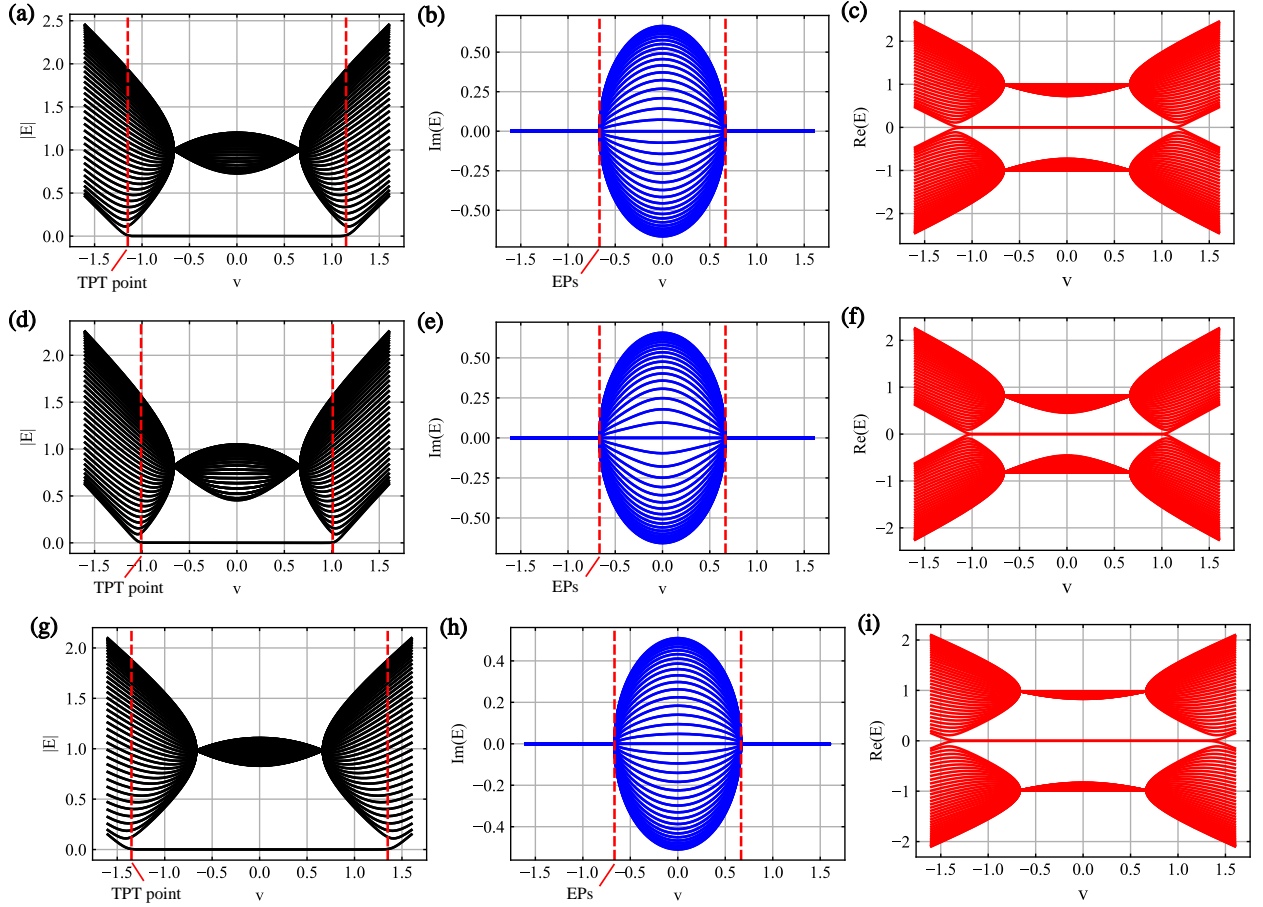


FIG. 2. Energy spectrum of the non-Hermitian SSH model coupled to a single mode cavity as a function of lattice intracell hopping strength v . (a) the amplitude $|E|$, (b) imaginary $\text{Im}(E)$ and (c) real $\text{Re}(E)$ part of energy spectrum in the absence of coupling to cavity ($g_{\text{coupling}} = 0$). (d) the amplitude $|E|$, (e) imaginary $\text{Im}(E)$ and (f) real $\text{Re}(E)$ part of energy spectrum in the presence of coupling to cavity ($g_{\text{coupling}} = 10$) with the intracell distance $b_0 = 0.2$. (g) the amplitude $|E|$, (h) imaginary $\text{Im}(E)$ and (i) real $\text{Re}(E)$ part of energy spectrum in the presence of coupling to cavity ($g_{\text{coupling}} = 10$) with the intracell distance $b_0 = 0.8$. Other parameters are chosen as intercell hopping strength $w = 1$, nonreciprocal intercell hopping strength $\gamma = 4/3$, number of unit cells $L = 40$, lattice constant $a_0 = 1$, cavity frequency $\omega_c = 0.15$, and maximum photon number in the Fock space $N_{\text{max}}^{\text{phot}} = 60$.

investigate the groundstate of the electron-dressed cavity and show that the SDS states can be obtained with high fidelity when there exists a \mathcal{PT} -symmetry phase transition in non-Hermitian SSH chain. To this extent we study the full Hamil-

tonian within a mean field ansatz assuming that there is no correlation between the photon ground state $|\phi\rangle$ and electronic ground state $|\varphi\rangle$. Thus, the photonic mean Hamiltonian reads

$$H_{\text{phot}} = \langle \varphi | H | \varphi \rangle = \left(v + \frac{\gamma}{2} \right) e^{i \frac{g_{\text{coupling}}}{\sqrt{L}} b_0 (a + a^\dagger)} D_{AB}^{jj} + \left(v - \frac{\gamma}{2} \right) e^{-i \frac{g_{\text{coupling}}}{\sqrt{L}} b_0 (a + a^\dagger)} (D_{AB}^{jj})^\dagger - w e^{i \frac{g_{\text{coupling}}}{\sqrt{L}} (1-b_0)(a + a^\dagger)} D_{AB}^{j+1,j} - w e^{-i \frac{g_{\text{coupling}}}{\sqrt{L}} (1-b_0)(a + a^\dagger)} (D_{AB}^{j+1,j})^\dagger + \omega_c (a^\dagger a + \frac{1}{2}), \quad (8)$$

where $D_{AB}^{jj} = \sum_{j=1}^L \langle \varphi | c_{j,A}^\dagger c_{j,B} | \varphi \rangle$ and $D_{AB}^{j+1,j} = \sum_{j=1}^{L-1} \langle \varphi | c_{j+1,A}^\dagger c_{j,B} | \varphi \rangle$ are the hopping matrix element in the electronic ground state $|\varphi\rangle$. By calculating the eigenvectors of the photonic Hamiltonian H_{phot} , we find the photon ground state $|\phi\rangle$. To see the quantum features of the

photon ground states, we now calculate the Wigner function. The Wigner function, as a phase-space quasiprobability distribution [3, 55], is defined in the (q, p) position and

momentum space as

$$W(q, p) = \frac{1}{2\pi} \int_{-\infty}^{\infty} dx \left\langle q - \frac{x}{2} \left| \rho \left| q + \frac{x}{2} \right\rangle e^{ipx}, \quad (9)$$

where ρ is the density matrix of the photon state $|\phi\rangle$.

As shown in Fig. 3(a) and Fig. 3(b), we plot the Wigner function of the photon ground state $|\phi\rangle$ and the exact SDSc state $|\phi^{SDSc}\rangle = S(r)D(\lambda)\left(\frac{|\alpha|+|- \alpha|}{\sqrt{2}}\right)$ in the \mathcal{PT} -symmetry phase of non-Hermitian SSH model ($v < \frac{\gamma}{2}$). $S(r) = \exp[(ra^\dagger - r^*a^2)/2]$ is the squeeze operator, $D(\lambda) = \exp(\lambda a^\dagger - \lambda^*a)$ is the displacement operator and $\frac{|\alpha|+|- \alpha|}{\sqrt{2}}$ is the Schrödinger-cat states. By comparing fig. 3(a) with fig. 3(b), we find that the phase-space quasiprobability distribution of $|\phi\rangle$ and $|\phi^{SDSc}\rangle$ are almost the same. Similar to Schrödinger's cat paradox, the presence of two peaks in the Wigner function in fig. 3(a) and fig. 3(b) corresponds to both the “dead cat” and the “alive cat” states, and the observation of negative values in the Wigner function signifies the nonclassical feature in SDSc state. We define the fidelity F between the photon ground (GS) states $|\phi\rangle$ in our system and the exact Squeezed Displaced Schrödinger-cat states state $|\phi^{SDSc}\rangle$ as

$$F = \text{Tr}[\sqrt{\sqrt{\rho_{SDSc}}\rho_{GS}\sqrt{\rho_{SDSc}}}], \quad (10)$$

where $\rho_{SDSc}(\rho_{GS})$ is the density matrix of the photon state $|\phi\rangle$ ($|\phi^{SDSc}\rangle$). As the fidelity F approaches 1, it indicates that the state generated by our system closely resembles the ideal state, show a high degree of similarity. After the numerical calculation, we find that the fidelity F between the photon ground state $|\phi^{GS}\rangle$ and the exact SDSc state $|\phi^{SDSc}\rangle$ is 0.994 revealing that the cavity ground state is steered into a SDSc state with high similarity.

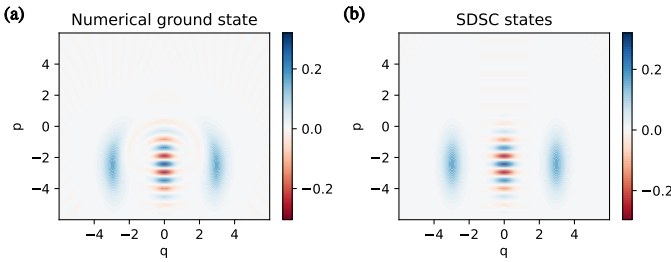


FIG. 3. Wigner function for (a) the photon ground state $|\phi\rangle$ and (b) the exact SDSc state $|\phi^{SDSc}\rangle = S(r)D(\lambda)\left(\frac{|\alpha|+|- \alpha|}{\sqrt{2}}\right)$ where $r = 0.54$, $\lambda = -i$ and $\alpha = 3.6$. Other parameters are chosen as intracell hopping strength $v = 1.3$, intercell hopping strength $w = 1$, nonreciprocal intercell hopping strength $\gamma = 8/3$, number of unit cells $L = 185$, intracell distance $b_0 = 0.9$, lattice constant $a_0 = 1$, cavity frequency $\omega_c = 0.15$, coupling strength $g_{coupling} = 11.1$, and maximum photon number in the Fock space $N_{max}^{phot} = 60$.

However, the fidelity F approaches 0 when the \mathcal{PT} symmetry of non-Hermitian SSH model recovers ($v \geq \frac{\gamma}{2}$). We showing this by plotting the fidelity F as functions of coupling strength $g_{coupling}$ and the intracell distance b_0 for different values of intracell hopping strength v in Fig. 4(a)-(c). Fig. 4(a)

shows a high fidelity in the area of large value b_0 , with a region of low fidelity in the remaining area of examined parameter when the \mathcal{PT} symmetry in non-Hermitian SSH chain is broken. Furthermore, from Fig. 4(a) we find that the SDSc state $|\phi^{SDSc}\rangle$ with high fidelity can be obtained with weaker coupling strength $g_{coupling}$ as the value of b_0 increased. When the \mathcal{PT} symmetry recovers ($v \geq \frac{\gamma}{2}$) the fidelity F approaches 0 although there exists maximum value of the fidelity F in Fig. 4(a) and 4(b). This implies a dramatic change in the ground state of the cavity $|\phi^{GS}\rangle$ in the presence of \mathcal{PT} symmetry of non-Hermitian SSH chain. We further show this by plotting the fidelity F in Fig. 4(d) as a function of intracell hopping strength v at fixed values of coupling strength $g_{coupling}$ and the intracell distance b_0 depicted. It can be vividly seen from Fig. 4(d) that the fidelity F approaches 1 as the \mathcal{PT} symmetry is broken ($v < \gamma/2$), undergoes an abrupt change at the EPs ($v = \gamma/2$), and ultimately decreases to 0 with the recover of the \mathcal{PT} symmetry. This implies that the emergency of the SDSc state can be regarded as a signature of the \mathcal{PT} -symmetry phase transition in the non-Hermitian SSH model. It is worth to note that the ground state of the cavity is no longer the SDSc state but a cavity state with the vanishing of two peaks and negative values in Wigner function with the recover of the \mathcal{PT} symmetry as depicted in the insets and it is an exact displaced squeezed vacuum state in the thermodynamic limit (see appendix D).

The cavity ground state corresponds to the state with the lowest eigenvalue of the electron-dressed cavity Hamiltonian. By examining the distribution of the Hamiltonian in phase space, we can gain insight into the physical mechanism underlying the alteration of the cavity ground state's properties. The cavity Hamiltonian can be conveniently described as a harmonic oscillator, allowing us to represent it using dimensionless position and momentum operators in the semiclassical limit $[x \equiv (a^\dagger + a)/2$ and $p \equiv (a^\dagger - a)/2i$. Thus, the semiclassical limit of Eq. (6) can be rewritten as

$$\begin{aligned} H_{\text{eff}}(x, p) &= \langle \varphi | H | \varphi \rangle \\ &= (v + \frac{\gamma}{2}) e^{i \frac{g_{coupling}}{\sqrt{L}} b_0 2x} D_{AB}^{jj} + (v - \frac{\gamma}{2}) e^{-i \frac{g_{coupling}}{\sqrt{L}} b_0 2x} (D_{AB}^{jj})^\dagger \\ &\quad - w e^{i \frac{g_{coupling}}{\sqrt{L}} (1-b_0) 2x} D_{AB}^{j+1, j} - w e^{-i \frac{g_{coupling}}{\sqrt{L}} (1-b_0) 2x} (D_{AB}^{j+1, j})^\dagger \\ &\quad + \omega_c (x^2 + p^2 + \frac{1}{2}), \end{aligned} \quad (11)$$

where $(x, p) \in \mathbb{R}^2$ are now continuous (nonquantized) classical variables. Therefore, the model described by a 1D tight-binding non-Hermitian SSH model coupled to a single mode cavity exhibits a semiclassical analogy with a single effective degree of freedom, and its phase space is denoted as $M = \mathbb{R}^2$. Mean-field properties of the quantum model Eq. (9) such as, e.g., the ground-state energy, the photon population can be captured by studying the distribution of energy of semiclassical Hamiltonian. Especially, the emergence of SDSc state $|\phi^{SDSc}\rangle$ can be understood through the structure of the classical phase space. In Fig. 5(a), 5(b) and 5(c), we show the

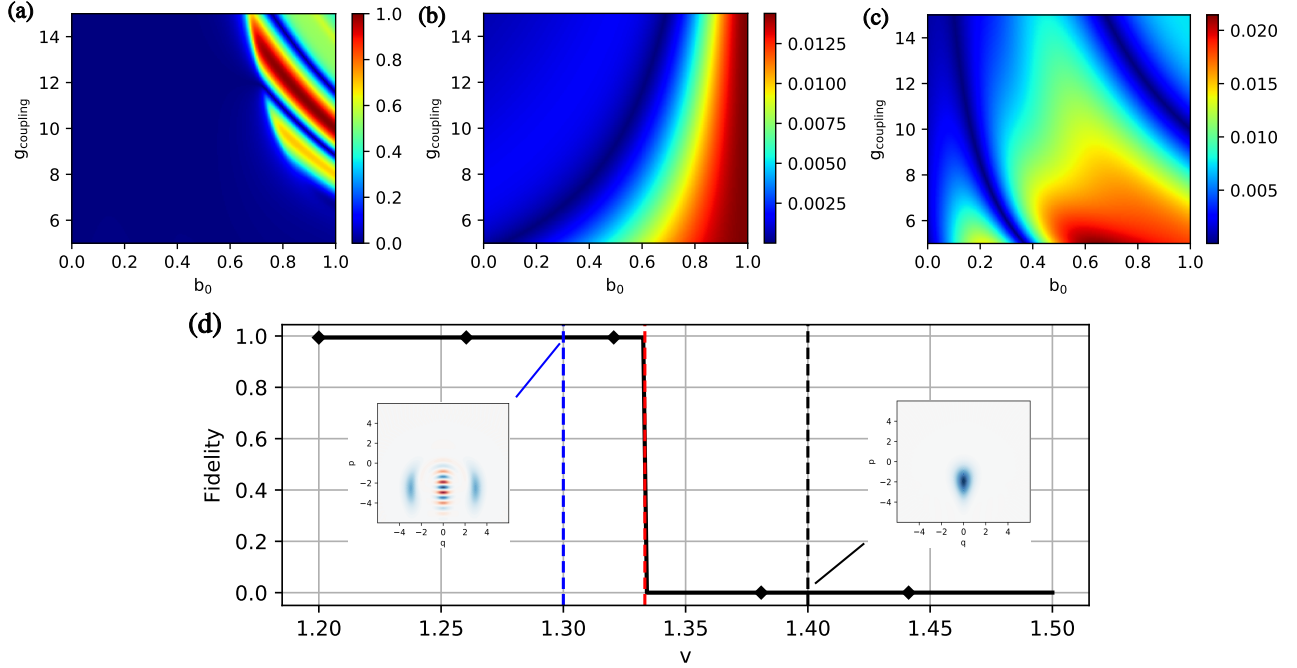


FIG. 4. Fidelity F between the photon ground (GS) states $|\phi^{GS}\rangle$ and the exact squeezed displaced Schrödinger-cat states $|\phi^{SDSc}\rangle$ as functions of coupling strength $g_{coupling}$ and intracell distance b_0 for (a) $\nu = 1.3$, (b) $\nu = \gamma/2$ and (c) $\nu = 1.4$. (d) Fidelity F as functions of ν when $g_{coupling} = 11.1$ and $b_0 = 0.9$, while the inset shows the Wigner function of cavity ground state at $\nu = 1.3$ (blue dashed line) and $\nu = 1.4$ (black dashed line). The red dashed line in (d) represents EPs ($\nu = \gamma/2$). Other parameters are chosen as intercell hopping strength $w = 1$, nonreciprocal intercell hopping strength $\gamma = 8/3$, number of unit cells $L = 185$, lattice constant $a_0 = 1$, cavity frequency $\omega_c = 0.15$ and maximum photon number in the Fock space is $N_{max}^{phot} = 60$.

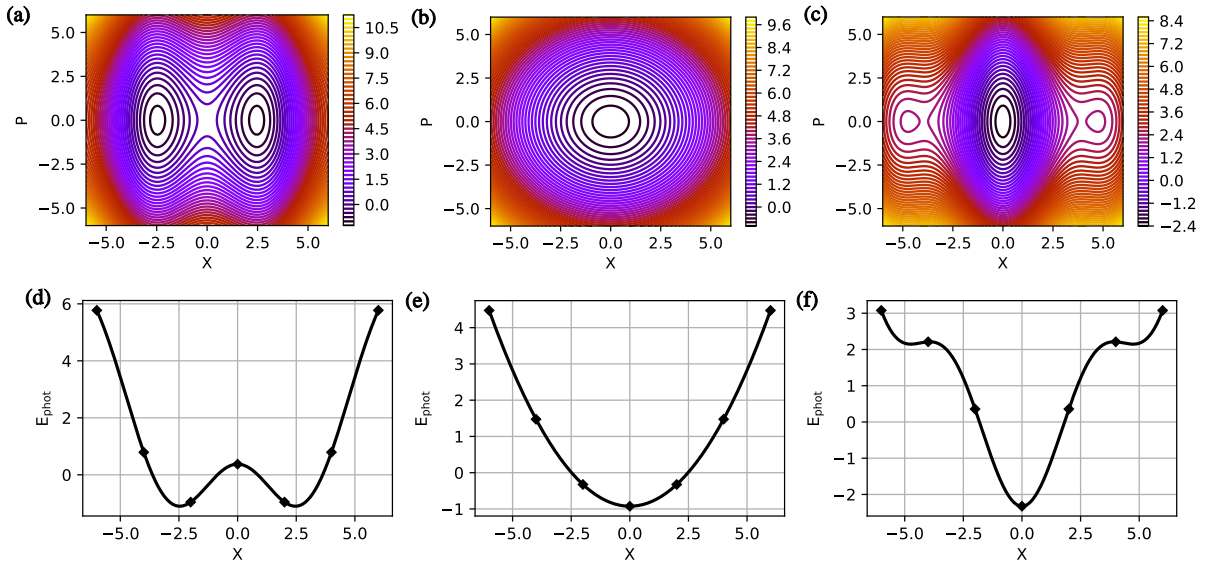


FIG. 5. Constant energy contours of the full classical Hamiltonian as functions of x and p for (a) $\nu = 1.3$, (b) $\nu = \gamma/2$ and (c) $\nu = 1.4$. Constant energy contours of the full classical Hamiltonian as functions of x when $p = 0$ for (d) $\nu = 1.3$, (e) $\nu = \gamma/2$ and (f) $\nu = 1.4$. Other parameters are chosen as intercell hopping strength $w = 1$, nonreciprocal intercell hopping strength $\gamma = 8/3$, number of unit cells $L = 185$, lattice constant $a_0 = 1$, cavity frequency $\omega_c = 0.15$, coupling strength $g_{coupling} = 11.1$ and maximum photon number in the Fock space is $N_{max}^{phot} = 60$.

energy contours of Hamiltonian Eq. (9), while the slice figure ($p = 0$) of energy are shown in Fig. 5(d), 5(e) and 5(f), accordingly. In Fig. 5(a), we observe that $H_{\text{eff}}(x, p)$ has global extrema at nonzero values of x and p . The classical phase space structure undergoes a complete transformation when $\mathcal{P}\mathcal{T}$ symmetry is broken ($v < \gamma/2$), revealing the emergence of two minima corresponding to the ground-state energy. These minima are positioned at symmetric values relative to $x = 0$ can be specifically shown in Fig. 5(d), and it makes the ground state of the cavity exhibits a distribution in phase space similar to that of a SDS state which is actually the two peaks in the Wigner function in Fig. 3(b). However, as shown in Fig. 5(b) and 5(e) when $v = \gamma/2$, $H_{\text{eff}}(x, p)$ allows for a single, global minimum at $x = p = 0$, corresponding to the ground-state energy. Although the energy of $H_{\text{eff}}(x, p)$ in Fig. 5(c) and 5(f) has local extrema at nonzero values of x and p , it has no connection with the ground-state energy and has no effect on cavity ground state. Therefore, one can see that phase-space quasiprobability distribution of cavity ground state in the presence of $\mathcal{P}\mathcal{T}$ symmetry has no two-peaks compared to that of SDS state due to the single, global minimum of energy at $x = p = 0$ when $v \geq \gamma/2$.

V. PHASE ESTIMATION WITH CAVITY GROUND STATE

The ground state, as the lowest energy eigenstate of the system, can be prepared as stable a quantum resource for quantum metrology without exciting a system to high energy level. In non-Hermitian systems, the $\mathcal{P}\mathcal{T}$ symmetry of the system may influence the ground state, as previously discussed, thereby impacting the quality of the ground state as a quantum resource. To this extend, we utilize the generated cavity ground states to estimate the phase in the optical interferometer and investigate the Quantum Fisher Information (QFI). Furthermore, the nonclassicality measured using an operational resource theory (ORT)[1] will be discussed.

As depicted in Fig. 6, the optical interferometer comprises two linear phase shifters, incorporating an unknown relative phase $\Phi_- = (\Phi_1 - \Phi_2)$ between the arms. The phase information will be encoded within the initial quantum state (cavity ground state $|\phi^{GS}\rangle$) at the input of the interferometer through unitary evolution, i.e.,

$$|\Psi\rangle = U_{\text{phase-shift}} |\Psi_0\rangle, \quad (12)$$

where $U_{\text{phase-shift}} = \exp[i(\Phi_1 a_1^\dagger a_1 + \Phi_2 a_2^\dagger a_2)]$, and $a_{1,2}^\dagger (a_{1,2})$ represent annihilation (creation) operators in the arms 1 and 2. $|\Psi_0\rangle = |\phi^{GS}\rangle \otimes |\phi^{GS}\rangle$ is the input state of the interferometer. Here, we concentrate on the relative phase between the two arms.

Considering a pure input state with path-symmetric, the unitary evolution can be simplified to $\exp[i\Phi_-(a_1^\dagger a_1 - a_2^\dagger a_2)/2]$. Then, the QFI of the unitary evolution of the initial state $|\Psi_0\rangle$ can be defined as[1]

$$F_{QFI} = 4 \langle \Psi_0 | \Delta^2 H | \Psi_0 \rangle, \quad (13)$$

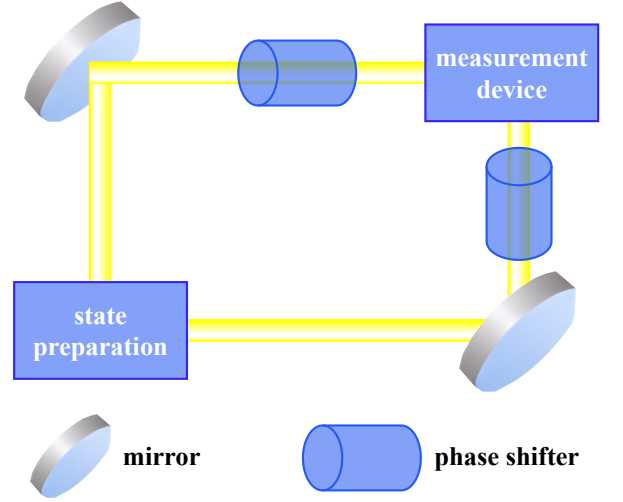


FIG. 6. An optical interferometer model is utilized for phase estimation. A prepared quantum state is input into the interferometer, where an unknown relative phase ($\Phi_1 - \Phi_2$) is introduced by two linear phase shifters between its arms. The phase information becomes encoded in the initial quantum state and is subsequently measured at the output ports. Other parameters are chosen as intercell hopping strength $w = 1$, intracell hopping strength $v = 1.3$, nonreciprocal intercell hopping strength $\gamma = 8/3$, number of unit cells $L = 185$, lattice constant $a_0 = 1$, cavity frequency $\omega_c = 0.15$, coupling strength $g_{\text{coupling}} = 11.1$, and maximum photon number in the Fock space is $N_{\text{max}}^{\text{phot}} = 60$.

where $H = i(\partial_{\Phi_-} U_{\text{phase-shift}}^\dagger) U_{\text{phase-shift}}$ and $\Delta^2 H = (H - \langle H \rangle)^2$. With the given operator $U_{\text{phase-shift}}$ expression, the QFI can be calculated as

$$F_{QFI} = 2[\text{Var}_{\Psi_0}(a_i^\dagger a_i) - \text{Cov}_{\Psi_0}(a_1^\dagger a_1, a_2^\dagger a_2)], i = 1 \text{ or } 2, \quad (14)$$

where $\text{Var}_{\Psi_0}(\cdot)$ and $\text{Cov}_{\Psi_0}(\cdot)$ are the variance and the covariance in the input state $|\Psi_0\rangle$, correspondingly. It can be clearly seen from Eq. (12) that QFI only depends on the properties of the input state ($|\phi^{GS}\rangle \otimes |\phi^{GS}\rangle$). Considering the initial state here is separable $\text{Cov}_{\Psi_0}(a_1^\dagger a_1, a_2^\dagger a_2) = 0$, thus the QFI can be reduced to $2\text{Var}_{\Psi_0}(a_i^\dagger a_i)$. In addition, a nonclassicality measure for quantum state rooted in the framework of ORT has been introduced, demonstrating various essential properties as a valuable resource for phase estimation. For pure states, nonclassicality measured based on ORT reads

$$N_n = \langle a^\dagger a \rangle - |\langle a \rangle|^2 + \left| \langle a \rangle - \langle a \rangle^2 \right|. \quad (15)$$

In order to study the impact of $\mathcal{P}\mathcal{T}$ symmetry on phase estimation utilizing the cavity ground state as a quantum resource, we plot the QFI F_{QFI} and the nonclassicality N_n as functions of intracell hopping strength v in Fig. 7(a) and 7(b), accordingly. From Fig. 7(a), a clear observation can be made that the value of QFI F_{QFI} is large as the $\mathcal{P}\mathcal{T}$ symmetry is broken ($v < \gamma/2$) which indicates that the cavity ground state is an appropriate quantum resource for phase estimation. However, there exists a sudden transition in value of F_{QFI} at the

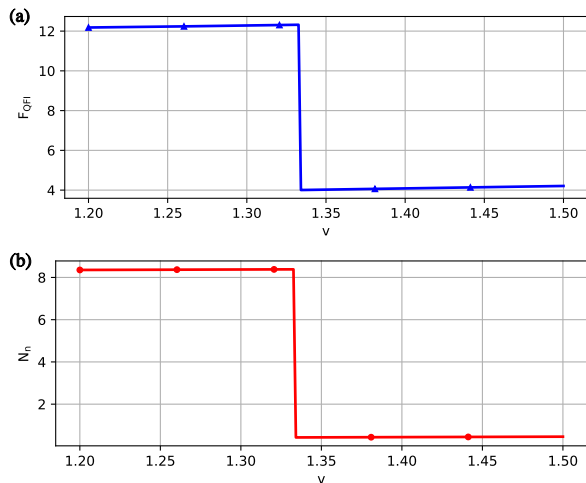


FIG. 7. (a) QFI F_{QFI} and (b) the nonclassicality N_n as functions of intracell hopping strength v . Other parameters are chosen as intercell hopping strength $w = 1$, nonreciprocal intercell hopping strength $\gamma = 8/3$, $g_{coupl} = 11.1$, $b_0 = 0.9$, number of unit cells $L = 185$, lattice constant $a_0 = 1$, cavity frequency $\omega_c = 0.15$, coupling strength $g_{coupling} = 11.1$, and maximum photon number in the Fock space is $N_{max}^{phot} = 60$.

exceptional point ($v = \sqrt{2}$), and it suddenly become small as the \mathcal{PT} symmetry recovers. Thus, the cavity ground state with \mathcal{PT} symmetry in non-Hermitian SSH model is not suitable for estimating phase. From Fig. 7(b), it is evident that the value of the nonclassicality N_n experiences a significant shift at the EPs. Simultaneously, the cavity ground state with broken \mathcal{PT} -symmetry exhibits higher nonclassicality, whereas the cavity ground state will lose some nonclassicality in the presence of \mathcal{PT} symmetry. Therefore, the ground state of the cavity can be viewed as a good quantum resource for phase estimation when \mathcal{PT} symmetry in non-Hermitian SSH

model is broken.

VI. CONCLUSION

In this work, we have investigated a non-Hermitian SSH chain coupled to a single spatially constant cavity mode. The open-boundary energy spectrum shows that topological phase transition in the non-Hermitian SSH chain can be modified by the fluctuation of cavity mode and captured in the photonic spectral function's behavior. However, \mathcal{PT} -symmetry phase transition can not be modified in the presence of cavity and is difficult to detect. Fortunately, the emergence of SDSc state with high fidelity can capture \mathcal{PT} -symmetry phase transition in non-Hermitian SSH model coupled to the quantum light field of a cavity. When \mathcal{PT} symmetry is broken the fidelity between exact SDSc state and cavity ground state approaches to almost 1, and then experiences a sharp drop to 0 as \mathcal{PT} symmetry recovers. The emergence of SDSc state can naturally be understood by inspecting the effective Hamiltonian $H_{eff}(x, p)$ in semiclassical limit: $H_{eff}(x, p)$ has local extrema at two sides of $x=0$ when \mathcal{PT} symmetry is broken. Therefore, our work therefore provides a convenient way to capture the \mathcal{PT} -symmetry phase transition in an electronic system. Besides, we exploit the ground state of cavity to estimate the phase in an optical interferometer, and find that QFI F_{QFI} and the nonclassicality N_n of the ground state will experience a sharp drop at the \mathcal{PT} -symmetry phase transition point. This indicates it is beneficial for quantum metrology and quantum information processing when considering the \mathcal{PT} -symmetry is broken in electronic system coupled to a cavity. Therefore, except for the flexible control and convenient probe of topological properties of the electronic systems provided by cavity photon, the ground state of cavity photon can be used to capture the \mathcal{PT} -symmetry phase transition in electronic system.

-
- [1] H. Markum, R. Pullirsch, and T. Wettig, Non-Hermitian Random Matrix Theory and Lattice QCD with Chemical Potential, Phys. Rev. Lett. 83, 484 (1999).
 - [2] N. Hatano and D. R. Nelson, Localization Transitions in Non-Hermitian Quantum Mechanics, Phys. Rev. Lett. 77, 570 (1996).
 - [3] M. Berry, Physics of Nonhermitian Degeneracies, Czech. J. Phys. 54, 1039 (2004).
 - [4] E. M. Graefe, H. J. Korsch, and A. E. Niederle, Mean-Field Dynamics of a Non-Hermitian Bose-Hubbard Dimer, Phys. Rev. Lett. 101, 150408 (2008).
 - [5] I. Rotter, A non-Hermitian Hamilton operator and the physics of open quantum systems, J. Phys. A: Math. Theor. 42, 153001 (2009).
 - [6] G. Barontini, R. Labouvie, F. Stubenrauch, A. Vogler, V. Guarerra, and H. Ott, Controlling the Dynamics of an Open Many-Body Quantum System with Localized Dissipation, Phys. Rev. Lett. 110, 035302 (2013).
 - [7] K. Jones-Smith and H. Mathur, Relativistic Non-Hermitian Quantum Mechanics, Phys. Rev. D 89, 125014 (2014).
 - [8] B. Ostahie and A. Aldea, Phosphorene confined systems in magnetic field, quantum transport, and superradiance in the quasiflat band, Phys. Rev. B 93, 075408 (2016).
 - [9] Y. Ashida, Z. Gong, and M. Ueda, Non-hermitian physics, Adv. Phys. 69, 249 (2020).
 - [10] C. Keller, M. K. Oberthaler, R. Abfalterer, S. Bernet, J. Schmiedmayer, and A. Zeilinger, Tailored Complex Potentials and Friedel's Law in Atom Optics, Phys. Rev. Lett. 79, 3327 (1997).
 - [11] C. M. Bender and S. Boettcher, Real Spectra in Non-Hermitian Hamiltonians Having PT Symmetry, Phys. Rev. Lett. 80, 5243 (1998).
 - [12] C. M. Bender, D. C. Brody, and H. F. Jones, Complex Extension of Quantum Mechanics, Phys. Rev. Lett. 89, 270401 (2002).
 - [13] A. Mostafazadeh, Pseudo-Hermiticity versus PT-symmetry. II. A complete characterization of non-Hermitian Hamiltonians with a real spectrum, J. Math. Phys. 43, 2814 (2002).

- [14] C. M. Bender, Making sense of non-Hermitian Hamiltonians, *Rep. Prog. Phys.* 70, 947 (2007).
- [15] A. Mostafazadeh, Pseudo-hermitian representation of quantum mechanics, *Int. J. Geom. Methods Mod. Phys.* 07, 1191 (2010).
- [16] K. Jones-Smith and H. Mathur, Non-Hermitian quantum Hamiltonians with PT symmetry, *Phys. Rev. A* 82, 042101 (2010).
- [17] R. El-Ganainy, K. G. Makris, M. Khajavikhan, Z. H. Musslimani, S. Rotter, and D. N. Christodoulides, Non-Hermitian physics and PT symmetry, *Nat. Phys.* 14, 11 (2018).
- [18] S. Klaiman, U. Günther, and N. Moiseyev, Visualization of Branch Points in PT-Symmetric Waveguides, *Phys. Rev. Lett.* 101, 080402 (2008).
- [19] Z. H. Musslimani, K. G. Makris, R. El-Ganainy, and D. N. Christodoulides, Optical Solitons in PT Periodic Potentials, *Phys. Rev. Lett.* 100, 030402 (2008).
- [20] Y. Chu, Y. Liu, H. Liu, and J. Cai, Quantum Sensing with a Single-Qubit Pseudo-Hermitian System, *Phys. Rev. Lett.* 124, 020501 (2020).
- [21] E. J. Bergholtz, J. C. Budich, and F. K. Kunst, Exceptional topology of non-Hermitian systems, *Rev. Mod. Phys.* 93, 015005 (2021).
- [22] S. Yao and Z. Wang, Edge States and Topological Invariants of Non-Hermitian Systems, *Phys. Rev. Lett.* 121, 086803 (2018).
- [23] X. M. Zhao, C. X. Guo, M. L. Yang, H. Wang, W. M. Liu, and S. P. Kou, Anomalous non-Abelian statistics for non-Hermitian generalization of Majorana zero modes, *Phys. Rev. B* 104, 214502 (2021).
- [24] Z. F. Yu, J. K. Xue, L. Zhuang, J. Zhao, and W. M. Liu, Non-Hermitian spectrum and multistability in exciton-polariton condensates, *Phys. Rev. B* 104, 235408 (2021).
- [25] X. M. Zhao, C. X. Guo, S. P. Kou, L. Zhuang, and W. M. Liu, Defective Majorana zero modes in a non-Hermitian Kitaev chain, *Phys. Rev. B* 104, 205131 (2021).
- [26] F. Yu, X. L. Zhang, Z. N. Tian, Q. D. Chen, and H. B. Sun, General Rules Governing the Dynamical Encircling of an Arbitrary Number of Exceptional Points, *Phys. Rev. Lett.* 127, 253901 (2021).
- [27] W. Y. Wang, B. Sun, and J. Liu, Adiabaticity in nonreciprocal Landau-Zener tunneling, *Phys. Rev. A* 106, 063708 (2022).
- [28] Y. Huang, Y. Shen, C. Min, S. Fan, and G. Veronis, Unidirectional reflectionless light propagation at exceptional points, *Nanophotonics* 6, 977 (2017).
- [29] S. Assaworrorarit, X. Yu and S. Fan, Robust wireless power transfer using a nonlinear parity-time-symmetric circuit, *Nature* 546, 387 (2017).
- [30] C. E. Rüter, K. G. Makris, R. El-Ganainy, D. N. Christodoulides, M. Segev and D. Kip, Observation of parity-time symmetry in optics, *Nat. Phys.* 6, 192 (2010).
- [31] B. Peng et al., Parity-time-symmetric whispering-gallery microcavities, *Nat. Phys.* 10, 394 (2014).
- [32] L. Chang, X. Jiang, S. Hua, C. Yang, J. Wen, L. Jiang, G. Li, G. Wang and M. Xiao, Parity-time symmetry and variable optical isolation in active-passive-coupled microresonators, *Nat. Photon.* 8, 524 (2014).
- [33] J. Schindler, A. Li, M. C. Zheng, F. M. Ellis and T. Kottos, Experimental study of active LRC circuits with PT symmetries, *Phys. Rev. A* 84, 040101 (2011).
- [34] C. M. Bender, B. K. Berntson, D. Parker and E. Samuel, Observation of PT phase transition in a simple mechanical system, *Am. J. Phys* 81, 173 (2013).
- [35] Karzig, T., Bardyn, C.-E., Lindner, N. H. & Refael, G. Topological polaritons. *Phys. Rev. X* 5, 031001 (2015).
- [36] Ohm, C. & Hassler, F. Microwave readout of majorana qubits. *Phys. Rev. B* 91, 085406 (2015).
- [37] Trif, M. & Tserkovnyak, Y. Resonantly tunable majorana polariton in a microwave cavity. *Phys. Rev. Lett.* 109, 257002 (2012).
- [38] Contamin, L. C., Delbecq, M. R., Douçot, B., Cottet, A. & Kontos, T. Hybrid light-matter networks of majorana zero modes. *npj Quant. Inform.* 7, 171 (2021).
- [39] Méndez-Córdoba, F. P. M. et al. Rényi entropy singularities as signatures of topological criticality in coupled photon-fermion systems. *Phys. Rev. Res.* 2, 043264 (2020).
- [40] Hübener, H. et al. Engineering quantum materials with chiral optical cavities. *Nat. Mater.* 20, 438–442 (2021).
- [41] Rokaj, V., Penz, M., Sentef, M. A., Ruggenthaler, M. & Rubio, A. Polaritonic hofstadter butterfly and cavity control of the quantized hall conductance. *Phys. Rev. B* 105, 205424 (2022).
- [42] Wang, X., Ronca, E. & Sentef, M. A. Cavity quantum electrodynamical chern insulator: towards light-induced quantized anomalous Hall effect in graphene. *Phys. Rev. B* 99, 235156 (2019).
- [43] Sentef, Michael A., et al. Quantum to classical crossover of Floquet engineering in correlated quantum systems. *Physical Review Research* 2.3 (2020): 033033.
- [44] Frisk Kockum, A., Miranowicz, A., De Liberato, S., Savasta, S. & Nori, F. Ultrastrong coupling between light and matter. *Nat. Rev. Phys.* 1, 19–40 (2019).
- [45] Dutra, S. M. Cavity quantum electrodynamics (John Wiley & Sons, Inc., 2004). <https://doi.org/10.1002/0471713465>.
- [46] Li, J. et al. Electromagnetic coupling in tight-binding models for strongly correlated light and matter. *Phys. Rev. B* 101, 205140 (2020).
- [47] Maissen, C. et al. Ultrastrong coupling in the near field of complementary split-ring resonators. *Phys. Rev. B* 90, 205309 (2014).
- [48] Meschede, D., Walther, H. & Müller, G. One-atom maser. *Phys. Rev. Lett.* 54, 551–554 (1985).
- [49] Thompson, R. J., Rempe, G. & Kimble, H. J. Observation of normal-mode splitting for an atom in an optical cavity. *Phys. Rev. Lett.* 68, 1132–1135 (1992).
- [50] Eckhardt, Christian J., et al. "Quantum Floquet engineering with an exactly solvable tight-binding chain in a cavity." *Communications Physics* 5.1 (2022): 122.
- [51] Bacciconi, Zeno, et al. "First-order photon condensation in magnetic cavities: A two-leg ladder model." *SciPost Physics* 15.3 (2023): 113.
- [52]

Appendix A: Mean-field method to decouple electrons and photons in finite-length non-Hermitian SSH chain in the presence of cavity

We present a detailed analysis of the solution to the light-matter Hamiltonian H Eq. (5) within the mean field approximation, which neglects correlations between cavity modes $|\phi\rangle$ and electrons $|\psi\rangle$.

$$|\Psi\rangle = |\psi\rangle|\phi\rangle. \quad (\text{A1})$$

Due to the mean field decoupling, we are tasked with solving an electronic mean field Hamiltonian as described by Eq. (6), alongside a photonic mean field Hamiltonian characterized expressed as Eq. (8). We determine the electronic spectrum of

the non-Hermitian SSH model in the presence of coupling to cavity photons through the self-consistent solution of Eq. (6) and Eq. (8). Specifically, we fix $g = 0$ in $H_{non-Hermitian-SSH}^{mf}$ and numerically compute $D_{AB}^{jj} = \sum_{j=1}^L \langle \varphi | c_{j,A}^\dagger c_{j,B} | \varphi \rangle$ and $D_{AB}^{j+1,j} = \sum_{j=1}^{L-1} \langle \varphi | c_{j+1,A}^\dagger c_{j,B} | \varphi \rangle$. Then we insert D_{AB}^{jj} and $D_{AB}^{j+1,j}$ into H_{phot} in Eq. (8) with $g \neq 0$, and evaluate v' , γ' and w' . Subsequently, we insert v' , γ' and w' (computed for $g \neq 0$) into $H_{non-Hermitian-SSH}^{mf}$, then insert them into $H_{non-Hermitian-SSH}^{mf}$ to calculate D_{AB}^{jj} and $D_{AB}^{j+1,j}$ again, and repeat the procedure until convergence. We find that the energy spectrum of the non-Hermitian SSH chain is modified in presence of cavity as shown in Fig. 2.

Appendix B: TPT in Non-Bloch Energy spectrum

In the electron lattices, the topological phase transition in the periodic boundary condition would be associated with a closing and reopening of the gap in the energy spectrum. Thus, we proceed to explore the energy spectrum under the periodic boundary condition, focusing on the occurrence of topological phase transitions. Before this, we note that the usual Bloch waves carry a pure phase factors e^{ik} where k is Bloch wave vector in Bloch Brillouin zone. However, the role of the phase factors e^{ik} is now played by $\beta = \sqrt{(v - \gamma/2)/(v + \gamma/2)} e^{ik}$ which has a modulus $|\beta| \neq 1$ in general. This allow us to write the Hamiltonian in non-Bloch Brillouin zone (see Methods). With the non-Bloch fermionic field $\psi_\beta^\dagger = (c_{\beta,A}^\dagger, c_{\beta,B}^\dagger)$, the renormalized Hamiltonian under the periodic boundary condition can be written in compact form as

$$H = \sum_{\beta} \psi_{\beta}^{\dagger} \frac{h(\beta)}{i\beta} \psi_{\beta} + \omega_c (a^{\dagger} a + \frac{1}{2}), \quad (\text{B1})$$

where the non-Bloch Hamiltonian $h(\beta)$ has this form

$$h(\beta) = \left[e^{-i \frac{g_{\text{coupling}}}{\sqrt{L}} b_0 (a + a^{\dagger})} (v - \gamma/2) + e^{i \frac{g_{\text{coupling}}}{\sqrt{L}} (1 - b_0) (a + a^{\dagger})} \beta w \right] \sigma^{-} + \left[e^{i \frac{g_{\text{coupling}}}{\sqrt{L}} b_0 (a + a^{\dagger})} (v + \gamma/2) + e^{-i \frac{g_{\text{coupling}}}{\sqrt{L}} (1 - b_0) (a + a^{\dagger})} \beta^{-1} w \right] \sigma^{+}, \quad (\text{B2})$$

where $\sigma^{\pm} = (\sigma_x \pm i\sigma_y)/2$ are pseudo-spin up(down) operator. In fact, the Hamiltonian of such a bipartite lattice can be written in the form of pseudo-spin components $h(\beta) = \sum_{i=x,y,z} d_{\beta i} \sigma_i$ by considering periodic boundary conditions. Here, at the first glance, it is apparent that the non-Bloch Hamiltonian $h(\beta)$ in Eq. (??) lacks the presence of an electronic mass term, i.e. $d_{\beta z} = 0$, indicating the preservation of chiral symmetry in the presence of cavity, i.e. $g \neq 0$. This guarantees the existence of eigenstate pairs with opposite energies.

By applying the mean-field method described in the previous section (see Methods), we perform calculations of the bulk energy spectrum while considering the interaction between electron and photons. Through the self-consistent solution of the electronic and photonic mean-field Hamiltonian, we observe that the influence of photons on the electronic hoppings which is characterized by purely real renormalization values $\xi(g, l)$, so the electronic bulk energy spectrum reads

$$\varepsilon = \pm \sqrt{R_+ R_-} = \pm \sqrt{(v')^2 - (\gamma')^2/4 + (w')^2 - 2w' \cos k \cdot \sqrt{(v' + \gamma'/2)(v' - \gamma'/2)}}, \quad (\text{B3})$$

where $R_{\pm} = (v' \pm \gamma'/2) + \beta^{\mp 1} w'$ are the pseudo-spin up(down) components of the non-Bloch Hamiltonian $h(\beta)$ with v' , γ' and w' defined before Eq. (B3). It is worth noting that ε is real at outside the EP point ($|v'| > |\gamma'/2|$).

Solving the photonic and electronic Hamiltonian self consistently we find numerically the Non-Bloch energy spectrum that we plot for three values of coupling strength g in Fig. 8 (panel (a) $g = 5$, panel (b) $g = 14$ and panel (c) $g = 20$). It is clear that there exists eigenstate pairs with opposite ener-

gies due to the preservation of chiral symmetry. Fig. 8(a) was exhibited to demonstrate a frequency gap between two bands when $g = 5$, but Fig. 8(b) incidentally shows that the gap is closed at the center of the Brillouin zone as $g = 14$, where they touch at Dirac points. When g is increased to 20, the gap is reopened with topological non-triviality which can be seen in the trajectories of R_{\pm} as shown in Fig. 8(d), (e) and (f). Figures 8(d) show that R_{\pm} have no wrapping to the origin and thus the electron system is topological trivial as $g = 5$. When

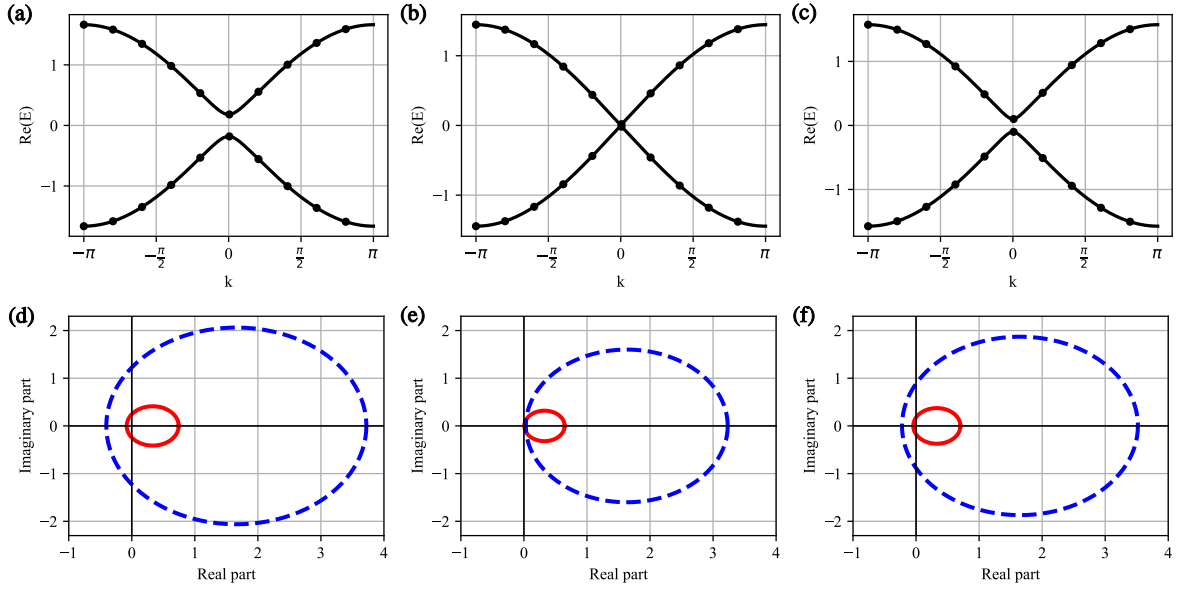


FIG. 8. Non-Bloch Energy spectrum ε in general brillouin zone with (a) $g = 5$, (b) $g = 14$ and (c) $g = 20$ correspondingly. Trajectories of R_{\pm} in ε with k in β running from 0 to 2π with (a) $g = 5$, (b) $g = 14$ and (c) $g = 20$ correspondingly. Other parameters are fixed as intercell hopping strength $w = 1$, nonreciprocal intercell hopping strength $\gamma = 4/3$, $b_0 = 0.2$, lattice constant $a_0 = 1$, cavity frequency $\omega_c = 0.15$, and maximum photon number in the Fock space $N_{\max}^{\text{phot}} = 60$.

g is increased to 14, the trajectories of R_{\pm} touch the origin and TPT happens. Then an anticlockwise and a clockwise wrappings to the origin are formed by R_+ and R_- , respectively, and thus the electron system is topological non-trivial as g increases across the value of 14. This gives a geometric picture to the TPT in Fig. 8(a), (b) and (c).

Appendix C: Photonic spectrum with topological phase transition

The excitation of electron in the non-Hermitian SSH system coupled to a cavity mode acts as hybrid light-matter polariton quasiparticles whose energies are affected by the topological phase transition in the electronic system. Meanwhile, the change in the properties of the polariton quasiparticles can be read out from a photonic spectrum which also unveils pivotal indications of the emission of the light from cavity. Thus, the topological property of the electronic system can be captured from the photonic spectrum. Particularly, we specifically investigate the photon spectral function $A(\omega) = -\frac{1}{\pi} \text{Im} \int dt e^{-i\omega t} (-i\theta(t)) \langle [a(t), a^\dagger] \rangle$ influenced by the electronic system, taking into account $1/L$ Gaussian fluctuations. By using photon Green's function method[] $A(\omega)$ can be expressed as

$$A(\omega) = -\frac{1}{\pi} \frac{\chi''(\omega)(\omega + \omega_c)^2}{(\omega^2 - \omega_c^2 - 2\omega_c \chi'(\omega))^2 + (2\omega_c \chi''(\omega))^2}, \quad (\text{C1})$$

where $\chi(\omega) = K(\omega) - \langle J_d \rangle$ is the current-current correlation function comprises both paramagnetic and diamagnetic con-

tributions, and $\chi'(\omega)$ ($\chi''(\omega)$) are the real (imaginary) part of $\chi(\omega)$ (see Methods),

$$\begin{aligned} K(\omega) &= \int_{-\infty}^{\infty} \langle T_c J_p(\tau) J_p(0) \rangle e^{i\omega\tau} d\tau, \\ J_p &= \frac{g}{\sqrt{L}} \sum_{\beta} \psi_{\beta}^{\dagger} (i\beta^{-1} w \sigma^+ - i\beta w \sigma^-) \psi_{\beta}, \\ J_d &= -\frac{g^2}{\sqrt{L}} \sum_{\beta} \psi_{\beta}^{\dagger} (\beta w \sigma^- + \beta^{-1} w \sigma^+) \psi_{\beta}, \end{aligned} \quad (\text{C2})$$

where $J_p(\tau)$ and $J_p(0)$ are the current operators in the Heisenberg picture. As depicted in Fig. 9, we illustrate the photonic spectral function's behavior in the presence of cavity. As shown in Fig. 9(a), in the topological trivial phase ($v > \sqrt{(w)^2 + (\gamma)^2/4}$), there only exists one peak in the photonic spectral function in the absence of cavity ($g_{\text{coupling}} = 0$), corresponding the cavity mode with frequency ω_c as depicted by the black dashed line. As the coupling strength g_{coupling} increasing, the peak splits into two branches indicating the appearance of the two hybrid light-matter polariton modes and the cavity mode with the frequency higher than $2E_{k=\pi}$ (white dashed line) can hybrid with the electron as shown in Fig. 9(b). As we fix the hopping parameters such that $v = \sqrt{(w)^2 + (\gamma)^2/4}$, the lowest branch of the photonic spectral function disappear revealing the absence of the polariton modes with the lowest frequency. This is directly linked to the closure of the bulk gap as depicted in Fig. 8(b), serving as a clear indication of the topological phase transition. When $v < \sqrt{(w)^2 + (\gamma)^2/4}$, that is topological non-trivial phase, the

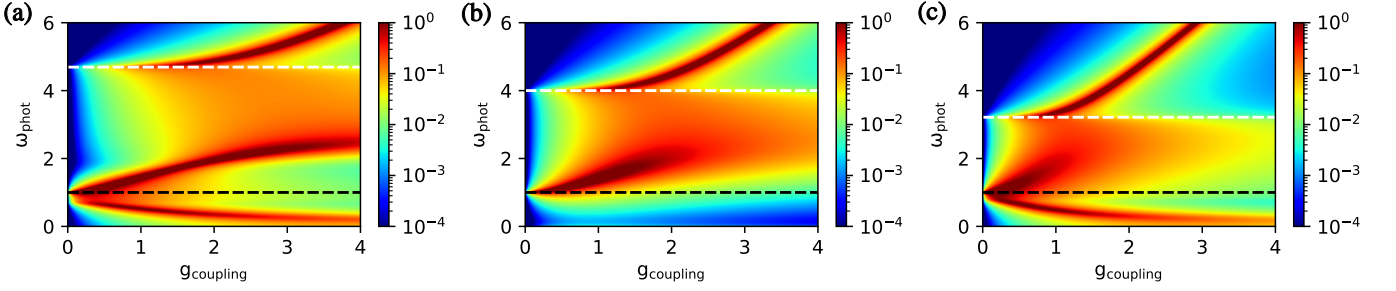


FIG. 9. Photonic spectral function as a function of the light-matter coupling g_{coupling} and photon frequency ω_{phot} . White dashed line corresponds to cavity frequency ω_c and black dashed line corresponds to $2E_{k=\pi}$ (the electronic bulk energy spectrum at $k = \pi$ in Eq. (10)). (a) intracell hopping $v = 1.5$ and intercell hopping $w = 1$ ($v > \sqrt{(w)^2 + (\gamma)^2/4}$) for topological trivial phase (b) $v = 1.2$ and $w = 1$ ($v = \sqrt{(w)^2 + (\gamma)^2/4}$) for TPT (c) $v = 0.9$ and $w = 1$ ($v < \sqrt{(w)^2 + (\gamma)^2/4}$) for topological non-trivial phase. Other parameters are fixed as nonreciprocal intercell hopping strength $\gamma = 4/3$, lattice constant $a_0 = 1$, cavity frequency $\omega_c = 1$, and maximum photon number in the Fock space $N_{\text{max}}^{\text{phot}} = 60$.

lowest branch of the photonic spectral function reappear indicating the reemergence of the lowest frequency polartion branch depicted in Fig. 9(c). Thus, the topological property of non-hermitian SSH chain can be probed by investigating the photonic spectral function's behavior in the presence of cavity.

Appendix D: Generation of displaced squeezed state

In addition to being able to generate squeezed displaced Schrödinger-cat states, other photonic states can emerge in the system where non-Hermitian SSH chain coupled to a single mode cavity. Therefore, we focus on the emergency of the displaced squeezed vacuum states. We expand H_{phot} in Eq. (8) to second order in the field that gave the only non-vanishing contribution in the thermodynamic limit to the ground state energy. It reads

$$H_{\text{phot}}^{2nd} = \omega_c (a^\dagger a + \frac{1}{2}) + \frac{g_{\text{coupling}}}{\sqrt{L}} (a + a^\dagger) \Pi - \frac{g_{\text{coupling}}^2}{2L} (a + a^\dagger)^2 \Lambda \quad (\text{D1})$$

where $\Lambda = (v + \frac{\gamma}{2}) D_{AB}^{jj} b_0^2 + (v - \frac{\gamma}{2}) (D_{AB}^{jj})^\dagger b_0^2 - w D_{AB}^{j+1,j} (1 - b_0)^2 - w (D_{AB}^{j+1,j})^\dagger (1 - b_0)^2$ and $\Pi = i(v + \frac{\gamma}{2}) D_{AB}^{jj} b_0 + i(v - \frac{\gamma}{2}) (D_{AB}^{jj})^\dagger b_0 - iw D_{AB}^{j+1,j} (1 - b_0) - iw (D_{AB}^{j+1,j})^\dagger (1 - b_0)$. It can

be diagonalized using a combined squeezing and displacement transformation

$$\begin{aligned} H^D &= e^{S^d[\Lambda, \Pi]} e^{S^{\text{sq}}[\Lambda]} H^{A, A^2} e^{-S^d[\Lambda, \Pi]} e^{-S^{\text{sq}}[\Lambda]} \\ S^d[\Lambda, \Pi] &= \frac{g_{\text{coupling}}}{\sqrt{L} \omega_0} \left(\frac{\mathcal{W}[\Lambda]}{\omega_0} \right)^{-\frac{3}{2}} (a^\dagger - a) \Pi, \\ S^{\text{sq}}[\Lambda] &= \frac{1}{4} \ln \left(\frac{\mathcal{W}[\Lambda]}{\omega_0} \right) (a^2 - (a^\dagger)^2). \end{aligned} \quad (\text{D2})$$

where $\mathcal{W}[\Lambda] = \omega_c \sqrt{1 - 2 \frac{g_{\text{coupling}}^2}{L \omega_c} \Lambda}$. Thus, the cavity ground state $|\phi^{GS}\rangle$ is given by the ground state of Hamiltonian H^D which is a displaced squeezed vacuum state $|\phi^{GS}\rangle^D$ that is connected to the bare cavity vacuum $|0\rangle$ through a combined squeezing and displacement transformation,

$$|\phi^{GS}\rangle^D = e^{S^d[\Lambda, \Pi]} e^{S^{\text{sq}}[\Lambda]} |0\rangle, \quad (\text{D3})$$

Therefore, we come to the fact that the cavity ground state is a displaced squeezed vacuum state in the thermodynamic limit when $\mathcal{P}\mathcal{T}$ symmetry is not broken.

